A numerical renormalization group approach to non-equilibrium Green functions for quantum impurity models

2008 J. Phys.: Condens. Matter 20 195216

(http://iopscience.iop.org/0953-8984/20/19/195216)

J. Phys.: Condens. Matter **20** (2008) 195216 (11pp) doi:10.1088/0953-8984/20/19/195216

A numerical renormalization group approach to non-equilibrium Green functions for quantum impurity models

Frithjof B Anders

Institut für Theoretische Physik, Universität Bremen, PO Box 330 440, D-28334 Bremen, Germany

E-mail: anders@itp.uni-bremen.de

Received 12 February 2008, in final form 20 March 2008
Published 11 April 2008
Online at stacks.iop.org/JPhysCM/20/195216

Abstract

We present a method for the calculation of dynamical correlation functions of quantum impurity systems out of equilibrium using Wilson's numerical renormalization group (NRG). Our formulation is based on a complete basis set of the Wilson chain and embeds the recently derived algorithm for equilibrium spectral functions. Our method fulfils the spectral weight conserving sum-rule exactly by construction. A local Coulomb repulsion $U > 0$ is switched on at $t = 0$, and the asymptotic steady-state spectral functions are obtained for various values of U as well as magnetic field strength H and temperature T. These benchmark tests show excellent agreement between the time-evolved and the directly calculated equilibrium NRG spectra for finite U. This method could be used for calculating steady-state non-equilibrium spectral functions at finite bias through interacting nanodevices.

(Some figures in this article are in colour only in the electronic version)

1. Introduction

Understanding the influence of the environment on the non-equilibrium dynamics of quantum systems remains one of the challenging questions of theoretical physics. A finite number of quantum mechanical degrees of freedom—an orbit, a spin or a qubit—interacting with an infinitely large bath of non-interacting bosons or fermions with a continuous energy spectrum represents a typical class of model examples for such systems.

These quantum impurity models appear to be at the heart of a variety of different physical problems. Traditionally, they were used to describe the interaction of magnetic impurities within a metallic host [1] or to investigate the dissipation in quantum mechanics [2]. These models have contributed immensely to our understanding of the low-temperature properties of single-electron transistors [3, 4] and the tunneling spectroscopy of adatoms on metal surfaces [5, 6]. In addition, within the dynamical mean-field theory [7, 8] or its cluster extensions [9] lattice models for strongly correlated fermions have been mapped onto quantum impurity problems embedded in a fictitious, self-consistent bath.

Many approaches to non-equilibrium are based on the Kadanoff–Baym [10] and Keldysh [11] techniques. At some time $t_0 = 0$ a closed system characterized by a density operator $\hat{\rho}_0$ evolves according to the Hamiltonian $\mathcal{H}(t)$. The immense difficulty of treating the real-time dynamics of quantum impurity systems stems from the need to track the full time evolution of the density operator of the entire system—environment plus impurity. The Kadanoff–Baym and Keldysh techniques [11, 10] provide an elegant platform for perturbative expansions of the density operator. One of the building blocks of such perturbative expansions are non-equilibrium Green functions. These non-equilibrium Green functions also contain information on the transients as well as the steady-state which might be reached in the long-time limit for a time-independent Hamiltonian. In general, however, perturbative approaches are plagued by the infra-red divergences caused by degeneracies on the impurity, making them inadequate for tackling the change of ground states of quantum impurity models [12].

In this paper, we present a different approach for the calculation of non-equilibrium Green functions of quantum impurity problems. We make use of Wilson's numerical renormalization group (NRG) method [12, 13] and its recent

extension to non-equilibrium dynamics [14, 15]. Spin–spin non-equilibrium spectral functions obtained by NRG calculations were investigated first by Costi about ten years ago in the context of the spin-boson model [16]. Here, we are interested in the evolution of fermionic spectral functions. We address this problem with a different approach using the complete basis set of the Wilson chain [12, 13] derived in the context of the time-dependent numerical renormalization group [14, 15] (TD-NRG). It has already been successfully applied to derive sum-rule conserving equilibrium Green functions [17, 18].

We focus on a quantum impurity system characterized by the thermodynamic density operator $\hat{\rho}_0 \propto \exp(-\beta\mathcal{H}^{\mathrm{i}})$ for times $t' < 0$. It evolves with respect to the Hamiltonian $\mathcal{H}^{\mathrm{f}}$ for times $t' \geqslant 0$. We will derive a closed analytical formula for any non-equilibrium Green function $G(t, t')$ for times $t, t' > 0$ given a time-independent $\mathcal{H}^{\mathrm{f}}$. In contrast to the equilibrium Green functions [18, 17], transitions between different energy shells require a double summation over pairs of Wilson shells (m, m'). In section 2.2, we prove that this summation can be cast into a recursion relation involving two different reduced density matrices instead of the single one used in the algorithm for equilibrium Green functions [18, 17]. It can be seen analytically that only one of these two reduced density matrices contributes if $\mathcal{H}^{\mathrm{i}} = \mathcal{H}^{\mathrm{f}}$: the equilibrium algorithm [18] is recovered. Therefore, the presented approach to non-equilibrium spectral functions embeds the equilibrium case [18, 17] as well.

We will heavily make use of this algorithm in another publication [19] on the current–voltage characteristics of interacting nanodevices. In that paper, we will derive a numerical renormalization group approach based on scattering states to describe current-carrying open quantum systems. In this formulation, the current at finite bias is determined by the steady-state non-equilibrium (NEQ) spectral function [20–23] which depends on the density operator of the full system. At finite bias, however, the NEQ density operator is only known analytically for Hamiltonians which commute with the number operators of left and right-moving electrons [21, 24], i.e. for non-interacting quantum impurities. This analytically known operator $\hat{\rho}_0$ must be evolved into the unknown NEQ density operator $\hat{\rho}$ after switching on a finite Coulomb repulsion U.

We have used the single-impurity Anderson model (SIAM) [25, 26] for benchmarking our algorithm. We have restricted ourselves to changes of local parameters of the quantum impurity at $t_0 = 0$. Consequently, the system has evolved with respect to the full Hamiltonian $\mathcal{H}^{\mathrm{f}}$. For an infinitely large bath, it is expected [10, 11, 24] that the initial $\hat{\rho}_0 \propto \exp(-\beta\mathcal{H}^{\mathrm{i}})$ evolved into the new thermodynamic density operator of the fully interacting problem described by $\mathcal{H}^{\mathrm{f}}$ for times $t \to \infty$, unless it is prohibited by some conservation law [24]. This is the basic underlying assumption of the perturbation theory in the Coulomb interaction U [27–29]. Therefore, the steady-state spectral function obtained from a time-evolved density operator should be equivalent to the spectra obtained directly by an equilibrium NRG calculation [25, 26, 18, 17].

We will use this comparison between both spectra as the benchmark for our algorithm in section 3. We will demonstrate excellent agreement between these differently calculated spectral functions for switching on the local Coulomb repulsion U from $U = 0$ to a finite value at various temperatures and local magnetic fields.

2. Theory

Interacting quantum dots, molecular junctions or other nanodevices are modeled by the interacting region $\mathcal{H}_{\mathrm{imp}}$, a set of non-interacting reservoirs $\mathcal{H}_{\mathrm{bath}}$ and a coupling between both subsystems $\mathcal{H}_I$

$$\mathcal{H} = \mathcal{H}_{\mathrm{imp}} + \mathcal{H}_{\mathrm{bath}} + \mathcal{H}_I. \tag{1}$$

We assume that the system is in equilibrium at times $t < 0$, and its properties are determined by the density operator $\hat{\rho}_0$. One possible choice would be $\mathcal{H}_I = 0$, which is usually the starting point of perturbative approaches based on the Keldysh formalism [11]. However, this is not required by our method. We only demand that the initial density operator can be cast in the form $\hat{\rho}_0 = \exp(-\beta\mathcal{H}^{\mathrm{i}})/Z$, where $\mathcal{H}^{\mathrm{i}}$ can be the initial Hamiltonian of the system in thermodynamic equilibrium for times $t < 0$.

At $t_0 = 0$, we suddenly switch from the Hamiltonian $\mathcal{H} = \mathcal{H}^{\mathrm{i}}$ to $\mathcal{H} = \mathcal{H}^{\mathrm{f}}$. The retarded two-time Green function,

$$\begin{aligned} G^r_{A,B}(t, t') &= -\mathrm{iTr}\left[\hat{\rho}_0[\hat{A}(t + t'), \hat{B}(t')]_{\mathrm{s}}\right]\Theta(t) \\ &= -\mathrm{iTr}\left[\hat{\rho}_0(t')[\hat{A}(t), \hat{B}]_{\mathrm{s}}\right]\Theta(t), \end{aligned} \tag{2}$$

contains information on the correlated dynamics of two operators $\hat{A}$ and $\hat{B}$, where

$$\hat{\rho}(t) = \mathrm{e}^{-\mathrm{i}\mathcal{H}^{\mathrm{f}}t}\hat{\rho}_0\mathrm{e}^{\mathrm{i}\mathcal{H}^{\mathrm{f}}t} \tag{3}$$

$$\hat{O}(t) = \mathrm{e}^{\mathrm{i}\mathcal{H}^{\mathrm{f}}t}O\mathrm{e}^{-\mathrm{i}\mathcal{H}^{\mathrm{f}}t}. \tag{4}$$

For fermionic operators the anti-commutator is used for $[\hat{A}(t), \hat{B}]_{\mathrm{s}}$ while for bosonic operators $[\hat{A}(t), \hat{B}]_{\mathrm{s}}$ represents a commutator. Equation (2) indicates that we can interpret such a two-time Green function as evolving the density operator of the system from $\tau = 0$ to the time $\tau = t'$, and calculating the correlation function of $\hat{B}$ and $\hat{A}$ with respect to the relative time $t > 0$. We expect that when changes are restricted to the local part of the Hamiltonian, i.e. $\mathcal{H}_{\mathrm{imp}} + \mathcal{H}_{\mathrm{I}}$, a steady state or even a new thermodynamic equilibrium [10, 11, 21, 24] is reached for times larger than the largest characteristic timescale of the system. In these cases, the limit

$$\hat{\rho}_\infty = \lim_{t'\to\infty}\hat{\rho}(t') \tag{5}$$

exists. Equation (2) becomes independent of t', and $G(t, t')$ only depends of the relative time t in the steady-state limit.

2.1. Complete basis set

Wilson's NRG method is a very powerful tool for accurately calculating equilibrium properties of quantum impurity models. Originally developed for treating the single-channel, single-impurity Kondo Hamiltonian [30, 12], this non-perturbative approach was successfully extended to the

Anderson impurity model [25, 26], and to the two-channel Anderson [31] and Kondo Hamiltonians [32, 33]. Recently, it was extended to equilibrium properties of impurity models with a *bosonic* bath [34, 35], non-equilibrium dynamics of the spin-boson model [15, 36] or even combinations of both fermionic and bosonic baths [37].

At the heart of this approach is a logarithmic discretization of the continuous bath, controlled by the discretization parameter $\Lambda > 1$; the continuum limit is recovered for $\Lambda \to 1$. Using an appropriate unitary transformation [12], the Hamiltonian is mapped onto a semi-infinite chain, defined by a sequence of finite-size Hamiltonians $\mathcal{H}_m$ with the impurity coupled to the open end. The iterations are terminated at a finite value of $m = N$ which defines the Wilson chain of finite length N. The finite-size Hamiltonian $\mathcal{H}_m$ acts only on the first m chain links of the Wilson chain. The length N also determines the temperature $T_N \propto \Lambda^{-N/2}$ for which the spectral functions are calculated. For a detailed review on this method see [13].

Recently, a *complete basis set* for such a Wilson chain of length N has been identified [14, 15]. The set of eigenstates of $\mathcal{H}_m$ can be formally constructed from the complete basis set $\{|\alpha_{\rm imp}, \alpha_0, \ldots, \alpha_N\rangle\}$ of the NRG chain of length N where the α_i label the configurations on each chain link i. Since $\mathcal{H}_m$ does not act on the chain links $m+1, \ldots, N$, an eigenstate $|r\rangle$ is written as $|r, e; m\rangle$ where the 'environment' variable $e = \{\alpha_{m+1}, \ldots, \alpha_N\}$ encodes the $N-m$ site labels $\alpha_{m+1}, \ldots, \alpha_N$. The index m is used in this notation to record where the chain is partitioned into a 'subsystem' and an 'environment'. After each iteration the eigenstates of $\mathcal{H}_m$ states are divided in 'discarded' and N_s 'kept' states. The standard NRG proceeds to the next iteration $m+1$ using only the kept states. It was proven [14, 15] that the discarded states from all NRG iterations, i.e. $\{|l, e; m\rangle_{\rm dis}\}$ also form a complete basis set. Regarding all eigenstates of the final NRG iteration as discarded, one can formally write the Fock space of the N-site chain in the form $\mathcal{F}_N = {\rm span}\{|l, e; m\rangle_{\rm dis}\}$, and the following completeness relation holds:

$$\sum_{m=m_{\rm min}}^{N} \sum_{l,e} |l, e; m\rangle_{\rm dis\ dis}\langle l, e; m| = 1. \tag{6}$$

Here the summation over m starts from the first iteration $m_{\rm min}$ at which a basis-set reduction is imposed. All traces below will be carried out with respect to this basis set. Hence, the evaluation of the spectral functions will not involve any truncation error. Note also that we made no reference to a particular Hamiltonian $\mathcal{H}$ in constructing the basis set $\{|l, e; m\rangle_{\rm dis}\}$.

At each iteration m, the Fock space $\mathcal{F}_N$ of a Wilson chain with fixed length N is partitioned by all previously discarded states

$$1_m^- = \sum_{m'=m_{\rm min}}^{m-1} \sum_{l',e'} |l', e'; m'\rangle_{\rm dis\ dis}\langle l', e'; m'|, \tag{7}$$

and all states present r at iteration m

$$\begin{aligned} 1_m^+ &= \sum_{m'=m}^{N} \sum_{l',e'} |l', e'; m'\rangle_{\rm dis\ dis}\langle l', e'; m'|. \\ &= \sum_{r,e} |r, e; m\rangle\langle r, e; m|. \end{aligned} \tag{8}$$

We will make extensive use of the completeness relation

$$1 = 1_m^- + 1_m^+ \tag{9}$$

in the following section.

2.2. Derivation of the NRG non-equilibrium Green function

For the moment, we will consider only the first term of the commutator of the retarded Green function $I(t', t) = {\rm Tr}\left[\hat{\rho}(t')\hat{A}(t)\hat{B}\right]$. If the operator $\hat{O}_t = \hat{A}(t)\hat{B}$ were a 'local' operator, i.e. an operator which only acts on impurity degrees of freedom or a Wilson chain of length $m_{\rm min}$ up to which all states are still maintained, we could use the TD-NRG [14, 15] to calculate the time evolution of $O_t(t') = {\rm Tr}\left[\hat{\rho}(t')\hat{O}_t\right]$.

In general, the time evolution of a local operator $\hat{O}$ leads to an operator $\hat{O}_t$ which acts on all chain degrees of freedom. Each operator $\hat{O}_t$ can always be expanded in outer products of all many-body states spanning the Fock space. Here, we will restrict ourselves always to a many-body Fock-space basis which is an approximate eigenbasis of the Wilson chain Hamiltonian. For the application of the TD-NRG, we require that the matrix elements of $\hat{O}_t$ remain diagonal in and independent of the environment degrees of freedom e, e'

$$\langle r, e; m|\hat{O}_t|s, e'; m\rangle = \delta_{e,e'} O^m_{rs}(t). \tag{10}$$

Then the operator qualifies as a local operator, as defined in equation (21) of [15]. We insert the completeness relation equation (9) between $\hat{A}(t)$ and $\hat{B}$ and obtain the two contributions

$$\begin{aligned} \langle r, e; m|\hat{A}(t)\hat{B}|s, e'; m\rangle &= \langle r, e; m|\hat{A}(t)(1_m^+ + 1_m^-)\hat{B}|s, e'; m\rangle \\ &= \sum_{k,e''} \langle r, e; m|\hat{A}(t)|k, e''; m\rangle\langle k, e''; m|\hat{B}|s, e'; m\rangle \\ &\quad + \sum_{m''=m_{\rm min}}^{m-1} \sum_{l'',e''} \langle r, e; m|\hat{A}(t)|l'', e''; m''\rangle_{\rm dis} \\ &\quad \times {}_{\rm dis}\langle l'', e''; m''|\hat{B}|s, e'; m\rangle. \end{aligned} \tag{11}$$

Restricting the operators $\hat{A}$ and $\hat{B}$ to local operators, the first term remains diagonal in e, e' [15]. In the second term, we again make use of equation (9), but partitioning the Fock-space of the Wilson chain with respect to iteration m'':

$$\begin{aligned} &\langle r, e; m|(1_{m''}^+ + 1_{m''}^-)\hat{A}(t)|l'', e''; m''\rangle_{\rm dis} \\ &\quad \times {}_{\rm dis}\langle l'', e''; m''|\hat{B}(1_{m''}^+ + 1_{m''}^-)|s, e'; m\rangle \\ &= \langle r, e; m|1_{m''}^+\hat{A}(t)|l'', e''; m''\rangle_{\rm dis} \\ &\quad \times {}_{\rm dis}\langle l'', e''; m''|\hat{B}\ 1_{m''}^+|s, e'; m\rangle \\ &= \sum_{k_1,e_1}\sum_{k_2,e_2} \langle r, e; m|k_1, e_1; m''\rangle\langle k_1, e_1; m''|\hat{A}(t)|l'', e''; m''\rangle_{\rm dis} \\ &\quad \times {}_{\rm dis}\langle l'', e''; m''|\hat{B}|k_2, e_2; m''\rangle\langle k_2, e_2; m''|s, e'; m\rangle \\ &= \sum_{k_1,e_1}\sum_{k_2,e_2} \langle r, e; m|k_1, e_1; m''\rangle A^{m''}_{k_1,l''} {\rm e}^{{\rm i}(E^{m''}_{k_1} - E^{m''}_{l''})t}\delta_{e_1,e''} \\ &\quad \times B^{m''}_{l'',k_2}\delta_{e_2,e''}\langle k_2, e_2; m''|s, e'; m\rangle\,. \end{aligned} \tag{12}$$

Note that $1_{m''}^-|s, e'; m\rangle = 0$ holds for $m'' < m$, and the indices k_1 and k_2 include all states present at iteration m'' as

seen from the definition of $1^{+}_{m''}$ in equation (8). The locality of the operators $\hat{A}$ and $\hat{B}$ has been used and leads to the condition $e_1 = e_2$. Since $m'' < m$, we can partition the environment degrees of freedom e_1 into $e_1 = (\tilde{e}_1, e'_1)$ where e'_1 labels the Wilson chain degree of freedom starting from chain link $m+1$. We obtain only non-zero matrix elements $\langle r, e; m|k_1, e_1; m''\rangle\langle k_2, e_1; m''|s, e'; m\rangle$, if $e = e'_1 = e'$. Therefore, equation (10) holds, and the matrix elements in equation (12) are independent of e.

Consequently, the operator $\hat{O}_t = \hat{A}(t)\hat{B}$ qualifies as a local operator in the sense of the TD-NRG [14, 15] for each time t, and $I(t', t)$ is given by the fundamental equation of the TD-NRG, equation (3) in [14],

$$I(t', t) = \sum_{m=m_{\min}}^{N} \sum_{r,s}^{\text{trun}} \mathrm{e}^{\mathrm{i}(E^m_r - E^m_s)t'} O^m_{r,s}(t)\rho^{\text{red}}_{s,r}(m). \tag{13}$$

Here $O^m_{r,s}(t) = \langle r, e; m|\hat{A}(t)\hat{B}|s, e; m\rangle$ is independent of e, and the reduced density matrix $\rho^{\text{red}}_{s,r}(m)$

$$\rho^{\text{red}}_{s,r}(m) = \sum_e \langle s, e; m|\hat{\rho}_0|r, e; m\rangle \tag{14}$$

is given in the NRG basis of $\mathcal{H}^{\text{f}}$. At each time t', the spectral information is encoded in the time evolution of $\hat{O}(t)$.

Inserting equation (11) into equation (13) yields two terms. The first contribution to $I(t, t_2)$ remains diagonal in the iteration index m and is given by the following expression

$$I_1(t', t) = \sum_{m=m_{\min}}^{N} \sum_{r,s}^{\text{trun}} \sum_k \mathrm{e}^{\mathrm{i}(E^m_r - E^m_s)t'} A^m_{r,k} \mathrm{e}^{\mathrm{i}(E^m_r - E^m_k)t} \times B^m_{k,s}\rho^{\text{red}}_{s,r}(m). \tag{15}$$

The restricted sum $\sum^{\text{trun}}_{r,s}$ requires that at least one of those indices r, s labels a discarded state at iteration m. The second contribution to $I(t', t) = I_1(t', t) + I_2(t', t)$, $I_2(t', t)$, contains a double summation over the iteration indices m and m''

$$I_2(t', t) = \sum_{m=m_{\min}}^{N} \sum_{r,s}^{\text{trun}} \sum_{m''=m_{\min}}^{m-1} \sum_e \mathrm{e}^{\mathrm{i}(E^m_r - E^m_s)t'} \times \sum_{l'',e''} \langle r, e; m|\hat{A}(t)|l'', e''; m''\rangle_{\text{dis dis}}\langle l'', e''; m''|\hat{B}|s, e; m\rangle \times \langle s, e; m|\hat{\rho}_0|r, e; m\rangle \tag{16}$$

which prevents a simple evaluation of the matrix elements of $\hat{A}$ and $\hat{B}$. Now, we insert equation (12) into equation (16) and arrive at

$$I_2(t', t) = \sum_{m=m_{\min}}^{N} \sum_{r,s}^{\text{trun}} \sum_{m''=m_{\min}}^{m-1} \sum_{k_1,k_2} \mathrm{e}^{\mathrm{i}(E^m_r - E^m_s)t'} \times \sum_{l'',e''} A^{m''}_{k_1,l''} \mathrm{e}^{\mathrm{i}(E^{m''}_{k_1} - E^{m''}_{l''})t} B^{m''}_{l'',k_2} \times \sum_{e,e_2} \langle r, e; m|k_1, e_2; m''\rangle\langle s, e; m|\hat{\rho}_0|r, e; m\rangle \times \langle k_2, e_2; m''|s, e; m\rangle. \tag{17}$$

The summation $\sum^N_{m=m_{\min}}$ and $\sum^{m-1}_{m''=m_{\min}}$ implies that $m'' < m$. Therefore, the summation can be arranged to

$$I_2(t', t) = \sum_{m''=m_{\min}}^{N-1} \sum_{l''}^{\text{trun}} \sum_{k_1} \sum_{k_2} A^{m''}_{k_1,l''}(t) B^{m''}_{l'',k_2} \times \tilde{\rho}^{\text{red}}_{k_2,k_1}(m'', t'), \tag{18}$$

where the indices k_1, k_2 run over all eigenstates of $\mathcal{H}_{m''}$ present at iteration m'', but the index l'' remains restricted to the discarded states. In the last step, we have defined a second reduced density matrix $\tilde{\rho}_{k_1,k_2}(m'', t')$ as

$$\tilde{\rho}_{k_2,k_1}(m'', t') = \sum_{m=m''+1}^{N} \sum_{r,s}^{\text{trun}} \sum_{e,e_1} \langle r, e; m|k_1, e_1; m''\rangle \times \langle k_2, e_1; m''|s, e; m\rangle\langle s, e; m|\hat{\rho}_0|r, e; m\rangle \times \mathrm{e}^{\mathrm{i}(E^m_r - E^m_s)t'}. \tag{19}$$

Partitioning the environment variable e_1 into $e_1 = (\alpha_{m''+1}, \cdots, \alpha_m, e')$, the relation

$$\tilde{\rho}^{\text{red}}_{k_2,k_1}(m'', t') = \sum_{m=m''+1}^{N} \sum_{r,s}^{\text{trun}} \sum_{\{\alpha_i\}} \rho^{\text{red}}_{s,r}(m)\mathrm{e}^{\mathrm{i}(E^m_r - E^m_s)t'} \times \langle r; m|k_1, \{\alpha_i\}; m''\rangle\langle k_2, \{\alpha_i\}; m''|s; m\rangle \tag{20}$$

is obtained. Here, we explicitly made use of the fact that the matrix elements $\langle k_2, e_1; m''|s, e; m\rangle$ are diagonal in e' and e and independent of e. The summation over e only enters the definition of $\rho^{\text{red}}_{s,r}(m)$.

Equation (20) connects $\tilde{\rho}^{\text{red}}_{k_2,k_1}(m, t')$ to all reduced density operators $\rho^{\text{red}}_{s,r}(m')$ from the later iterations $m' > m$. If $\tilde{\rho}^{\text{red}}_{k_2,k_1}(m+1, t')$ is given, $\tilde{\rho}_{k_2,k_1}(m, t')$ obeys the following recursion relation

$$\begin{aligned}\tilde{\rho}^{\text{red}}_{k_2,k_1}(m, t') &= \sum_{r,s}^{\text{trun}} \sum_{\alpha_{m+1}} \langle k_2, \alpha_{m+1}; m|s; m+1\rangle \\ &\times \left[\rho^{\text{red}}_{s,r}(m+1)\mathrm{e}^{\mathrm{i}(E^{m+1}_r - E^{m+1}_s)t'}\right]\langle r; m+1|k_1, \alpha_{m+1}; m\rangle \\ &+ \sum_{k',k''}^{\text{trun}} \sum_{\alpha_{m+1}} \langle k_2, \alpha_{m+1}; m|k'; m+1\rangle \\ &\times \tilde{\rho}^{\text{red}}_{k',k''}(m+1, t')\langle k''; m+1|k_1, \alpha_{m+1}; m\rangle\end{aligned} \tag{21}$$

which we have obtained from equation (20). We initialize this recursion with $\tilde{\rho}^{\text{red}}_{k',k''}(N, t') = 0$. Defining the auxiliary matrix

$$\rho'_{r,s}(m+1, t') = \rho^{\text{red}}_{s,r}(m+1)\mathrm{e}^{\mathrm{i}(E^{m+1}_r - E^{m+1}_s)t'} + \tilde{\rho}_{k',k''}(m+1, t'), \tag{22}$$

the recursion relation (21) has the same structure as equation (40) of [15].

Note that the overlap matrix elements $\langle k_2, \alpha_{m+1}; m|k'; m+1\rangle$ are identical to the matrix elements $A^{\alpha_{m+1}}_{k',k2}$ as defined in equation (2) of [17]. Matrix elements of this type $\langle r; m|k_1, \{\alpha_i\}; m''\rangle$ can be evaluated directly using a product of $m - m''$ such A-matrices [17].

At each recursion step $\rho'_{r,s}(m+1, t')$ involves two terms which contribute matrix elements to different sectors of ρ'. By construction, $\tilde{\rho}_{k',k''}(m+1, t)$ has only non-zero matrix elements for k' and k'' being both retained states of the NRG iteration $m+1$.

The restricted sum over r and s projects out the other sectors of the matrix $\rho'_{r,s}(t') = \rho^{\text{red}}_{s,r}(m+1, t') + \tilde{\rho}_{s,r}(m+1, t')$ for which at least one of the indices s, r labels a discarded state. Instead of a single reduced density matrix, we need to keep track of two matrices at each iteration, namely $\rho^{\text{red}}_{r,s}(m)$ and $\tilde{\rho}^{\text{red}}_{r,s}(m, t')$.

Then, the two contributions to $I(t', t)$ read

$$I(t', t) = \sum_{m=m_{\min}}^{N} \sum_{r,s}^{\text{trun}} \sum_{k} \mathrm{e}^{\mathrm{i}(E_r^m - E_s^m)t'} A_{r,k}^m \mathrm{e}^{\mathrm{i}(E_r^m - E_k^m)t} \times B_{k,s}^m \rho_{s,r}^{\text{red}}(m) + \sum_{m=m_{\min}}^{N-1} \sum_{l'}^{\text{trun}} \sum_{k_1} \sum_{k_2} A_{k_1,l'}^m \mathrm{e}^{\mathrm{i}(E_{k_1}^m - E_{l'}^m)t} B_{l',k_2}^m \times \tilde{\rho}_{k_2,k_1}^{\text{red}}(m, t'). \quad (23)$$

This formally requires only a single summation over m: the second summation over m' has been absorbed into the definition of $\tilde{\rho}_{k_2,k_1}^{\text{red}}(m, t')$. Note that the index l' labels all discarded states at iteration m. Obviously, the same type of calculation must also be performed for the second term of the commutator in equation (2) in order to obtain all contributions for the Green function. Fourier transformation of equation (23) with respect to t yields the spectral information of interest.

It has to be emphasized that only energetic approximations have been made. The NRG truncation influences the partitioning of the states, but the completeness of the basis is always guaranteed [14, 15]. Therefore, the spectral sum-rule remains fulfilled exactly for each time t' as in the equilibrium case [18]. It is straightforward to apply our algorithm also to the lesser and greater Green functions $G^<(t, t')$ and $G^>(t, t')$ as discussed in [17].

2.3. Steady-state limit

For all systems in which a time-independent steady-state density operator $\hat{\rho}_\infty$ is reached, equation (5) becomes equivalent to

$$\hat{\rho}_\infty = \lim_{T\to\infty} \frac{1}{T} \int_0^T \mathrm{d}\tau \hat{\rho}_0(\tau). \quad (24)$$

This formulation is particularly useful for a discretized representation of an infinitely large system since artificial finite-size oscillations are averaged out. The steady-state limit of the two-time Green function,

$$G_\infty^r(t) = \lim_{t'\to\infty} G_{A,B}^r(t, t') = -\mathrm{i}\mathrm{Tr}\left[\hat{\rho}_\infty [A(t), B]_\mathrm{s}\right] \Theta(t), \quad (25)$$

is obtained using equations (23) and (24) by noting that

$$\lim_{T\to\infty} \frac{1}{T} \int_0^T \mathrm{d}\tau \mathrm{e}^{\mathrm{i}(E_r^m - E_s^m)\tau} = \delta_{E_\mathrm{r}, E_\mathrm{s}}. \quad (26)$$

In the first part of equation (23) as well as in the recursion relation (21), the reduced density matrix $\rho_{s,r}^{\text{red}}(m)$ contributes only energy diagonal matrix elements. In general, however, the reduced density matrix $\tilde{\rho}_{k,k'}^{\text{red}}$ will not be diagonal in the NRG eigenbasis.

We introduce the integral $L_{A,B}(t')$ of the Fourier transformed Green function $G_{A,B}^r(\omega, t')$ with respect to t as

$$L_{A,B}(t') = -\int_{-\infty}^{\infty} \frac{\mathrm{d}\omega}{\pi} \mathrm{Im}\, G_{A,B}^r(\omega, t'). \quad (27)$$

For operators $\hat{A}$ and $\hat{B}$, whose anti-commutator—commutator for bosonic operators—remains constant, $L_{A,B}(t')$ defines a sum-rule independent of t' which is fulfilled exactly by our approach at any time t' due to the usage of a complete basis set. Therefore, the averaged sum-rule

$$L_{A,B} = \lim_{t'\to\infty} L_{A,B}(t') = -\lim_{T\to\infty} \frac{1}{T} \int_0^T \mathrm{d}\tau \times \int_{-\infty}^{\infty} \frac{\mathrm{d}\omega}{\pi} \mathrm{Im}\, G_{A,B}^r(\omega, \tau) \quad (28)$$

remains exactly fulfilled as well. An example would be the single-particle spectral function obtained from equation (23) by setting $A = f_\sigma$ and $B = f_\sigma^\dagger$. In this case $L_{f_\sigma, f_\sigma^\dagger}(t') = 1$. In fact, we used this criterion to check explicitly the sum-rule conservation and found that it remains always within machine precision with an error of 10^{-15} independent of all parameters.

A word is in order about the usage of the term 'steady-state'. We expect that a steady-state is always reached at long times for a time-independent Hamiltonian [24] $\mathcal{H}^\mathrm{f}$ in quantum impurity systems. In a closed but infinite quantum system, where only $\mathcal{H}_\mathrm{imp} + \mathcal{H}_I$ has been changed, the steady-state will be identical to the thermodynamic equilibrium described by the density operator $\hat{\rho} = \exp(-\beta\mathcal{H}^\mathrm{f})/Z_\mathrm{f}$, in the sense that all local expectation values calculated with ρ_∞ and $\hat{\rho}$ will be the same. It requires that the limit $\lim_{t'\to\infty} \lim_{V\to\infty}$ is taken such that $t' \ll V$ in appropriate dimensionless units.

A steady-state rather than a thermodynamic equilibrium [21, 24] will be reached for an open quantum system in the limit $t' \to \infty$ [21, 24] at finite bias. Again, it requires that the limit $\lim_{t'\to\infty} \lim_{V\to\infty}$ is taken in the correct order. However, within a discretized representation of such a quantum impurity system, we can never distinguish between the approach to a true thermodynamic equilibrium and non-equilibrium steady-state for times $t' \to \infty$. Therefore, we will always use the term 'steady-state' throughout the paper even for situations where it can be proven that the corresponding continuum limit of the model approaches the thermodynamic limit for infinitely long times [24]. In fact, the difference between our steady-state and equilibrium spectral function will serve as a criterion for the quality of our approach.

2.4. Recovering the sum-rule conserving equilibrium NRG Green function

Equation (23) must contain all contributions to the equilibrium Green function [17, 18] as well. In equilibrium, the initial and final Hamiltonian are identical ($\mathcal{H} = \mathcal{H}^\mathrm{i} = \mathcal{H}^\mathrm{f}$), the density operator $\hat{\rho}_0$ commutes with $\mathcal{H}$. The overlap matrix $S_{r,s}$ between eigenstates of $\mathcal{H}^\mathrm{i}$ and $\mathcal{H}^\mathrm{f}$, $S_{r,s} = {}_i\langle s; m | r, m\rangle_f$ must be diagonal. Then, I_1 contributes with an energy diagonal $\rho_{s,r}^{\text{red}}(N)$ only on the last Wilson shell and is identical to equation (11) of [18]. For $m < N$, $\rho_{s,r}^{\text{red}}(N)$ has only non-zero matrix elements for r and s being a kept state, which are explicitly excluded by the summation restriction. Therefore, $\rho_{s,r}^{\text{red}}(m)$ contributes only once to the reduced density matrix $\tilde{\rho}_{k_2,k_1}^{\text{red}}(m, t')$ in the recursion relation equation (21), namely at iteration $N - 1$. As a consequence, the reduced density matrix $\tilde{\rho}_{k_2,k_1}^{\text{red}}(m, t')$ becomes

time independent in equilibrium and equal to the reduced density matrix $\rho^{\rm red}_{k_2,k_1}(m)$, i.e. $\tilde{\rho}^{\rm red}_{k_2,k_1}(m,t') = \rho^{\rm red}_{k_2,k_1}(m)$. The Fourier transformation of $I_2(t'=0,t)$ with respect to t yields equation (16) of [18].

2.5. The non-equilibrium NRG algorithm

As in the equilibrium NRG [12], each chain length N corresponds to a temperature $T_{\rm N} \propto \Lambda^{-N/2}$. For $\mathcal{H}^{\rm i}$ and $\mathcal{H}^{\rm f}$, two simultaneous NRG runs are performed in order to generate the density operator $\hat{\rho}_0$ using $\mathcal{H}^{\rm i}$ and the eigenenergies of $\mathcal{H}^{\rm f}$ for the time evolution. At each iteration m, we calculated the overlap matrix $S_{r,r'}(m)$ between all eigenstates r of $H^{\rm f}_m$ and all eigenstates r' of $\mathcal{H}^{\rm i}_m$ [15]. This information, as well as the unitary matrices diagonalizing $\mathcal{H}^{\rm i}_m$ and $\mathcal{H}^{\rm f}_m$ are stored. At the end of the NRG runs, the equilibrium density matrix [12–15] is calculated using the last iteration of $H^{\rm i}_N$:

$$\hat{\rho}_0 = \frac{1}{Z_{\rm N}} \sum_l {\rm e}^{-\beta_{\rm N} E^N_l} |l;\, N\rangle\langle l;\, N| \tag{29}$$

where $Z_{\rm N} = \sum_l \exp(-\beta_{\rm N} E^N_l)$.

We have implemented the TD-NRG algorithm [15] recursively by going backwards from m to $m-1$. For each backward iteration, we perform the following steps:

(i) calculate the reduced density matrix in the basis of $\mathcal{H}^{\rm i}_m$ using equation (40) in [15]
(ii) calculate $\rho'_{r,s}(m+1,t')$ according to equation (22)
(iii) calculate $\tilde{\rho}^{\rm red}_{r,s}(m,t')$ using the recursion equation (21)
(iv) combine $\tilde{\rho}^{\rm red}_{r,s}(m,t')$ and $\rho^{\rm red}_{r,s}(m+1)$ to a single reduced density matrix
(v) evaluate the contribution of iteration m to the excitation spectrum obtained by Fourier transform equation (23)
(vi) steps (i)–(v) are repeated until we reach the iteration $m_{\rm min}$ at which no state was eliminated.

While the selection of retained states in the NRG run for $\mathcal{H}^{\rm i}$ is determined by the density matrix [12], the selection of states of $\mathcal{H}^{\rm f}$ is guided by the notion of maximizing the overlap with the eigenstates of $\mathcal{H}^{\rm i}$. Amongst the different truncation schemes that we have implemented, the simplest was the most effective [14, 15]. In this truncation scheme, we selected the lowest eigenstates of $\mathcal{H}^{\rm f}_m$ at the end of each iteration m as well.

In [19] the current through a nanodevice coupled to two leads is investigated as a function of the finite applied bias using the algorithm for the NEQ spectral function presented here. The device is described by a two-band model. Each band representing the bath continuum for either left or right-moving scattering states will be set to a different chemical potential μ_α, $\alpha = {\rm L}, {\rm R}$. The potential different $V = \mu_{\rm R} - \mu_{\rm L}$ drives a finite current through the nanodevice. In this case, the NRG run for $\mathcal{H}^{\rm i}$ obtains a faithful many-body representation of the density operator of the non-interaction problem ($U = 0$)

$$\hat{\rho}_0 \propto {\rm e}^{-\beta(\mathcal{H}^{\rm i} - \hat{Y}_0)} \tag{30}$$

where operator [21]

$$\hat{Y}_0 = \sum_\alpha \mu_\alpha N_\alpha \tag{31}$$

replaces the usual number operator for a grand canonical ensemble in order to include the different potentials μ_α of the scattering states.

After each iteration for $\mathcal{H}^{\rm f}_m$, one would like to retain the states with the largest overlap with the eigenstates of $\mathcal{H}^{\rm i}_m$. These eigenstates of $\mathcal{H}^{\rm f}$ are generally expected to be connected to the eigenstates of $\mathcal{H}^{\rm i}$ of the same eigenenergy relative to the ground state by the Lippmann–Schwinger equation for a model with a continuous bath. In practice, we select those eigenstates of $\mathcal{H}^{\rm f}_m$ which have the lowest diagonal matrix elements of the operator $\mathcal{H}^{\rm f}_m - \hat{Y}_0$. Therefore, the eigenenergies $E_{\rm s}$ of $\mathcal{H}^{\rm f}_m$ can be divided into two contributions

$$E_{\rm s} = \Delta E_{\rm s} + \sum_\alpha \mu_\alpha n^s_\alpha. \tag{32}$$

The first term $\Delta E_{\rm s}$ is of the order $\Lambda^{-m/2}$ due to the truncation scheme, and the second term is defined by

$$\langle s|\hat{Y}_0|s\rangle = \sum_\alpha \mu_\alpha n^s_\alpha = \sum_\alpha \mu_\alpha \langle s|\hat{N}_\alpha|s\rangle. \tag{33}$$

The question of the distribution and magnitude of the excitation energies $\Delta E_{\rm rs} = E^m_{\rm r} - E^m_{\rm s}$ entering equation (23) arises in order to understand the redistribution of spectral weight at finite bias. $\Delta E_{\rm rs}$ involves eigenenergies of $\mathcal{H}^{\rm f}_m$ and is given by

$$\Delta E_{\rm rs} = \Delta E_{\rm r} - \Delta E_{\rm s} + \sum_\alpha \mu_\alpha \left(n^r_\alpha - n^s_\alpha\right). \tag{34}$$

The single-particle spectral function is obtained from equation (23) by setting $A = f_\sigma$ and $B = f^\dagger_\sigma$. Only those states r and s can contribute to the spectral function whose total number of particles differs by exactly one electron, i.e.

$$\sum_\alpha \left(n^r_\alpha - n^s_\alpha\right) = \pm 1. \tag{35}$$

Substituting equation (35) into (34) yields the two equivalent ways of writing the excitation energies

$$\Delta E_{\rm rs} = \Delta E_{\rm r} - \Delta E_{\rm s} + (\mu_{\rm R} - \mu_{\rm L})\left(n^r_{\rm R} - n^s_{\rm R}\right) \pm \mu_{\rm L} \tag{36}$$

$$= \Delta E_{\rm r} - \Delta E_{\rm s} + (\mu_{\rm L} - \mu_{\rm R})\left(n^r_{\rm L} - n^s_{\rm L}\right) \pm \mu_{\rm R}. \tag{37}$$

For models with a channel conservation law, $|(n^r_\alpha - n^s_\alpha)| = 0, 1$ must hold. As a consequence, the excitation energies $\Delta E_{\rm rs}$ are centered around the two chemical potentials μ_α. For interacting quantum impurity models which violate channel conservation [21, 19], the differences $|\Delta N^{rs}_\alpha|$ are given by arbitrary numbers. By inserting a finite value of $(n^r_\alpha - n^s_\alpha)$ into equation (36) or (37), it becomes apparent that the energy difference $\Delta E_{\rm rs}$ will be shifted away from either chemical potential by multiples of the chemical potential differences $V = \mu_{\rm L} - \mu_{\rm R}$ [21, 19].

A word is in order concerning the frequency resolution. In the usual equilibrium NRG the lowest resolvable frequency [13] coincides with the temperature $T_{\rm N} \propto \Lambda^{-N/2}$ set by the length of the Wilson chain. The non-equilibrium Green functions $G(t,t')$ depend on two different times. The Fourier transformation with respect to relative time t remains meaningful even in the limit $t' \to \infty$, since the steady-state

density operator $\hat{\rho}_\infty$ exists and is well defined by equation (24). However, the smallest excitation energy resolved might be larger than $\omega_N \approx \Lambda^{-N/2}$ due to the difference between $\hat{\rho}_\infty^{\text{TD-NRG}}$ obtained via equation (24) and the exact steady-state density operator for a bath continuum. Depending on the bias V and values of U, the lower boundary for frequency resolution increases to $\omega_{\text{low}} \approx \Lambda^{-m/2}$ which typically changes $m = N-1$ to $m = N-3$. In all cases, we investigated in [19], the bias V remains significantly larger than ω_{low}.

3. Results

3.1. The single-impurity Anderson model

In order to demonstrate the potential of this approach, we will present results for the single-particle spectral functions of the single-impurity Anderson model (SIAM) for which the equilibrium spectral functions are well studied [38–40, 13, 18] and can serve as benchmarks.

The Hamiltonian of the SIAM [41, 25, 26]

$$\mathcal{H} = \sum_{k\sigma} \epsilon_{k\sigma} c_{k\sigma}^\dagger c_{k\sigma} + H_{\text{imp}} + V \sum_{k\sigma} \left(c_{k\sigma}^\dagger f_\sigma + f_\sigma^\dagger c_{k\sigma} \right) \tag{38}$$

$$\begin{aligned} \mathcal{H}_{\text{imp}} &= \mathcal{H}_0 + \mathcal{H}_U \\ &= \sum_\sigma \left(\epsilon_{\text{f}} + \frac{U}{2} - \frac{\sigma}{2} H \right) f_\sigma^\dagger f_\sigma + \frac{U}{2} \left(\sum_\sigma n_\sigma^{\text{f}} - 1 \right)^2 \\ &= \sum_\sigma \left(\epsilon_{\text{f}} - \frac{\sigma}{2} H \right) f_\sigma^\dagger f_\sigma + U n_\uparrow^{\text{f}} n_\downarrow^{\text{f}} \end{aligned} \tag{39}$$

$$\mathcal{H}_U = \frac{U}{2} \left(\sum_\sigma n_\sigma^{\text{f}} - 1 \right)^2 \tag{40}$$

consists of a single local state, which we will denote by f, with energy ϵ_{f} and Coulomb repulsion U, coupled to a bath of conduction electrons with creation operators $c_{k\sigma}^\dagger$ and energies $\epsilon_{k\sigma}$. The local level is subject to a Zeeman splitting in an external magnetic field H. Note that the single-particle term of the impurity Hamiltonian $\mathcal{H}_{\text{imp}}$ can be written in two different ways, i.e. the last two lines of equation (39) which allows for a conventional interaction term—last line of equation (39)—or a non-interaction term containing the Hartree contribution and a particle–hole preserving interaction term $\mathcal{H}_U$ [25, 26]. To obtain a continuous spectral function from the set of discrete δ-functions occurring in $G_{A,B}(z)$, the occurring $\delta(\omega - \omega_n)$ functions are replaced by a Gaussian broadening on a logarithmic mesh

$$\delta(\omega - \omega_n) \to \frac{\text{e}^{-b^2/4}}{b\omega_n\sqrt{\pi}} \exp\left\{ -\left(\frac{\ln(\omega/\omega_n)}{b} \right)^2 \right\} \tag{41}$$

where b ranges typically between $0.6 \leqslant b < 1.2$ [42, 18, 13].

The Fourier transformation of the Green function $G_{A,B}^r(t,t')$ with respect to t obeys the equation of motion

$$z G_{A,B}^r(z,t') = \text{Tr}\left[\hat{\rho}(t')[A, B]_s \right] + G_{[H,A],B}^r(z,t') \tag{42}$$

for any time t' and a time-independent Hamiltonian $\mathcal{H}^{\text{f}}$. (Note that a time-dependent $\mathcal{H}^{\text{f}}(t)$ yields the usual integral equation, and equation (42) would not hold.)

By setting $A = f_\sigma$ and $B = f_\sigma^\dagger$, Bulla *et al* derived a simple but exact relation between two Green functions and the correlation self-energy [39]

$$\Sigma_\sigma^U(z,t') = U \frac{G^r_{f_\sigma n_{-\sigma}, f_\sigma^\dagger}(z,t')}{G^r_{f_\sigma, f_\sigma^\dagger}(z,t')} \tag{43}$$

which is used to express the retarded Green function as

$$\begin{aligned} G^r_{f_\sigma, f_\sigma^\dagger}(z,t') &= \left[z - \epsilon_{\text{f}} - \frac{\sigma}{2} H - \Delta_\sigma(z) - \Sigma_\sigma^U(z,t') \right]^{-1}, \\ \Delta_\sigma(z) &= \frac{1}{N} \sum_k \frac{V^2}{z - \epsilon_{k\sigma}}. \end{aligned} \tag{44}$$

We have calculated the Green functions $G^{r(NRG)}_{f_\sigma n_{-\sigma}, f_\sigma^\dagger}(z,t')$ and $G^{r(NRG)}_{f_\sigma, f_\sigma^\dagger}(z,t')$ in the steady-state limit $t' \to \infty$ and have obtained the physical Green function via the equation of motion (44) and (43).

As long as not otherwise stated, all energies are measured in units of $\Gamma = \pi V^2 \rho(0)$, and a constant band width [12] of $\rho(\omega) = 1/(2D)\Theta(D - |\omega|)$ is used with $D/\Gamma = 20$. The number of kept states after each NRG iteration was $N_{\text{s}} = 2000$. To check the accuracy, we calculated the sum-rule of the raw NRG spectral function by integrating the δ-peaks analytically and confirmed that for arbitrary parameters and number of states the sum-rule for the steady-state spectral function is fulfilled within a machine precision of 10^{-15}. The algorithm itself combines the time-dependent NRG [14, 15] implementation with the calculation of the sum-rule conserving spectral functions as discussed elaborately in [18].

3.2. Particle–hole symmetry

3.2.1. External magnetic field $H = 0$. In figure 1, the steady-state spectral functions for a particle–hole symmetric regime are compared with the equilibrium solution obtained directly from the standard NRG procedure [18]. In these calculations, the Hartree term $U/2$ has been absorbed into $\mathcal{H}^{\text{i}}$. At time $t' = 0$, the Coulomb interaction $\mathcal{H}_U$ is switched on. An excellent agreement between the equilibrium NRG result (dashed lines) and the long-time limit of the time-evolved spectral functions (solid lines) is found. The non-interacting resonant-level spectral function centered around $\omega = 0$ evolves continuously into the Green function for a SIAM with finite U. The inset in figure 1 shows small deviations between the reference equilibrium spectra for $\mathcal{H} = \mathcal{H}^{\text{f}}$ and the steady-state spectra obtained from the Fourier transform of equation (25) in the Kondo regime. Note that the exponentially small Kondo scale not accessible to perturbation theories in U is always accounted for correctly within the NRG and, therefore, in our algorithm by the crossover to the fixed-point spectrum of $\mathcal{H}^{\text{f}}$ [25, 26]. With increasing values of U and fixed Λ, the peak height decreases from its theoretical unitary limit of $1/(\pi\Gamma)$. The deviations are less that 1% for $U = 2$ and increase to approximately 11% for $U = 10$. The correct low-energy scale [25, 13] T_{K} proportional to the width of the resonance at $\omega = 0$ emerges as well in the steady-state spectral functions.

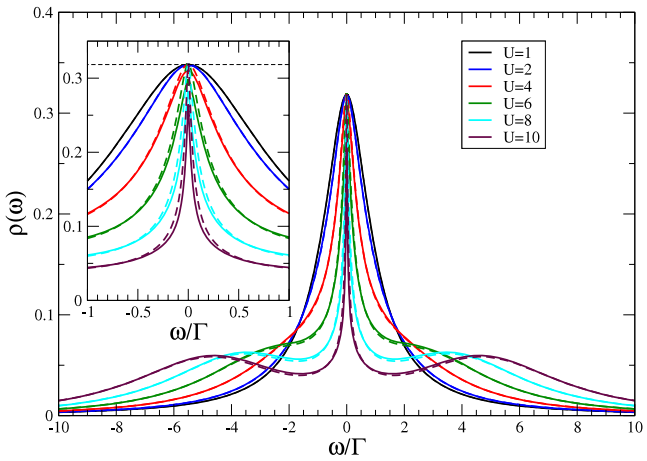

Figure 1. Comparison of the spectral function for the six different values of U for the symmetric case $\epsilon_f = -U/2$. The steady-state spectral function, obtained from switching $\mathcal{H}_U = 0$ to a finite value is plotted as a straight line, while the direct equilibrium calculation [18] is given by dashed lines of the same color for the same parameters. The inset shows the resonance in the vicinity of the chemical potential. The dashed line in the inset indicates the unitary limit of $1/(\pi\Gamma)$. NRG parameters: $\Gamma/D = \pi V^2\rho_0/D = 0.05$, $\Lambda = 2$, $N_S = 2000$, $b = 0.6$, $T \to 0$.

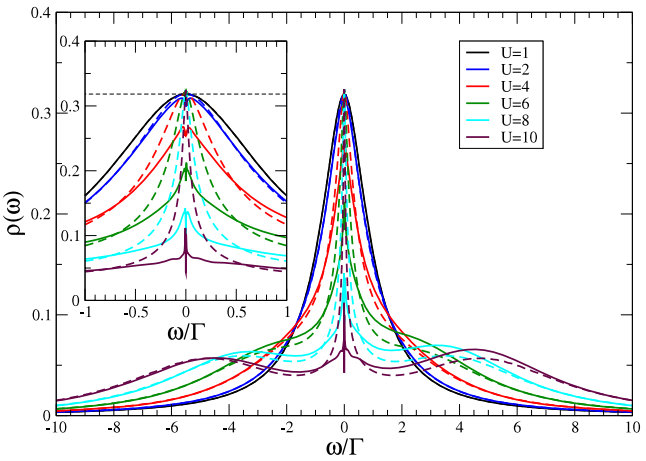

Figure 2. Comparison of the spectral function for the six different values of U for the symmetric case $\epsilon_f = -U/2$. The Hartree term $U/2$ is absent in the Hamiltonian of $\mathcal{H}^i$, and the Coulomb interaction $H_U = Un^f_\uparrow n^f_\downarrow = \mathcal{H}^f - \mathcal{H}^i$ is switched on at $t' = 0$. The steady-state spectral functions are plotted as solid lines, while the direct equilibrium calculation [18] yields the dashed lines for the same parameters. The colors (color online) are identical for the same values of U. The inset shows the resonance in the vicinity of the chemical potential. NRG parameters: as in figure 1.

We investigated also the impact of the initial level position ϵ^i_f on the steady-state spectra. A different starting point for $U = 0$ could be the traditional way of writing the impurity Hamiltonian $\mathcal{H}_{\rm imp} = \sum_\sigma(\epsilon_f - \frac{\sigma}{2}H) f^\dagger_\sigma f_\sigma + Un^f_\uparrow n^f_\downarrow$ which is identical to (39). Here, the Hartree term $U/2$ is not absorbed into the single-particle energy and the Coulomb repulsion term $\mathcal{H}_U = Un^f_\uparrow n^f_\downarrow$ is switched on at $t' = 0$.

The results for this starting point are presented in figure 2. The steady-state spectra show an increasing deviation from the correct thermodynamic equilibrium spectrum which remains pinned at $1/\pi$ for all values of U in accordance with the density of state sum-rule [43, 44]. All steady-state spectra remain particle–hole symmetric, guaranteed by $\mathcal{H}^f$, and the high-energy features are well reproduced. However, we observe deviations from the correct Abrikosov–Suhl resonance (ASR) even for moderate values of $U > 2\Gamma$. For large values of U, the ASR is almost absent in the steady-state spectra.

The difference can be understood in the following way. By absorbing the Hartree term into the initial Hamiltonian $\mathcal{H}^i$, the average impurity occupation $\langle n_f\rangle$ does not change with time. $\mathcal{H}^i$ and $\mathcal{H}^f$ will flow to the same strong-coupling fixed point for $T \to 0$. The excellent agreement between the equilibrium reference spectrum and the steady-state spectrum can be seen in figure 1.

In figure 2, however, we have started with a non-interacting Hamiltonian which breaks particle–hole symmetry: the level position is located at $\epsilon_f = -U/2$. For increasing values of $U/\Gamma > 1$, it corresponds to a doubly occupied level as the starting configuration while the final spectra must be particle–hole symmetric for $\epsilon_f = -U/2$. The strong-coupling fixed point of $\mathcal{H}^i$ is characterized by an additional marginal operator which is proportional to the strength of the particle–hole symmetry breaking [26]. For energies larger than the characteristic energy scale T_K, a good agreement is found for the high-energy parts of the spectrum which is determined mainly by the mean occupation. However, the low-energy spectrum, which contains information on the many-body resonance, deviates increasingly with increasing values of U from the reference curve.

3.2.2. Finite external magnetic field. The particle–hole symmetry, present at $H = 0$ is broken at a finite magnetic field. In figure 3(a), a comparison is shown between the equilibrium spectral functions (dashed lines) and $\rho(\omega, t' \to \infty)$ obtained after switching on a finite value of U in a fixed and finite magnetic field of $H = 0.2$. The position and height of the many-body resonance is well reproduced. The small deviations for the equilibrium values increase with increasing value of U. A shift in spectral weight from negative to positive frequencies of the majority spectrum at large values of U indicates a slight underestimation of the spin-polarization for values of $U \geqslant 8$. Due to the total spin conservation of the Hamiltonian, a relaxation of the total magnetization is prohibited. This is the source of additional small deviations [14, 15] besides discretization errors in the finite-size representation of the infinitely large system.

Alternatively, we have kept U fixed and switched on a finite magnetic field H at $t' = 0$, as depicted in figure 3 (b). Again, the equilibrium spectra are well reproduced by $\rho(\omega, t' \to \infty)$.

3.3. Particle–hole asymmetric regime

The influence of the initial level position ϵ^i_f on the steady-state spectra is depicted in figure 4 for local particle–hole asymmetric parameters $\epsilon^f_f = -2.4$ and $U = 8$. Again, we start initially with $U = 0$. For variation of ϵ^i_f which

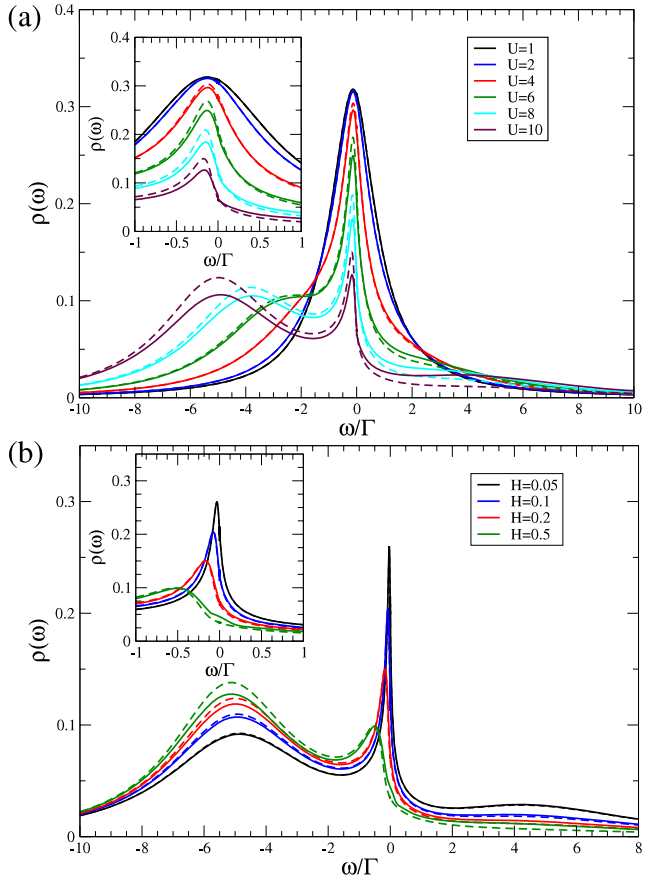

Figure 3. Comparison (a) of the majority spin spectral function for the six different values of U for the symmetric case $\epsilon_f = -U/2$ at a fixed finite magnetic field $H = 0.2$. The color coding and NRG parameters are identical to those in figure 1. The steady-state spectral functions, obtained by switching $\mathcal{H}_U = 0$ to a finite value are plotted as straight lines, while the direct equilibrium calculation [18] is given by the dashed lines with the same color for the same $\mathcal{H}^f$. In (b) $U/\Gamma = 8$ and $\epsilon_f/\Gamma = -4$ has been kept constant while the external magnetic field is switched on. The inset shows the resonance in the vicinity of the chemical potential. NRG parameters: as in figure 1.

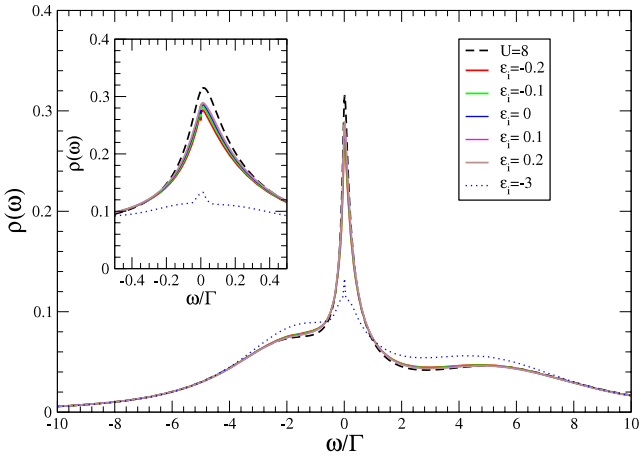

Figure 4. Influence of the initial value of the level position in $\mathcal{H}^i$ on the steady-state spectrum for a fixed value of $U = 8$. The initial level position ϵ_f has been set to $\epsilon_f^i/\Gamma = -3, -0.2, -0.1, 0, 0.1, 0.2$. The black dashed line shows the equilibrium NRG spectra for the small parameters as $\mathcal{H}^f$. The inset shows the resonance in the vicinity of the chemical potential. NRG parameters: as in figure 1.

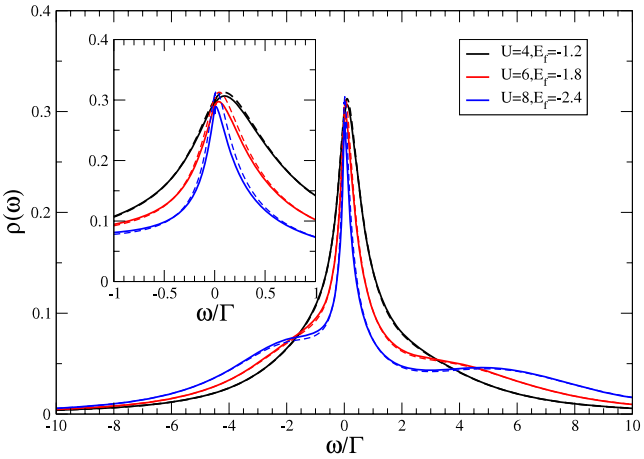

Figure 5. Comparison of the spectral function for the three different values of U for the asymmetric case. The initial level position ϵ_f has been set to $\epsilon_f^i = 0.235, 0.21, 0.175$ and $\epsilon_f^f = -2.4$. The inset shows the resonance in the vicinity of the chemical potential. NRG parameters: as in figure 1.

changes the level occupancy n_f very moderately, the steady-state spectral function shows only marginal changes. We observe a significant deviation from the equilibrium NRG spectral function only for a large negative initial value of $\epsilon_f^i/\Delta = -3$, for which the impurity is essentially doubly occupied. Although the shape and position of the high-energy excitation maxima are well reconstructed in this case, the strongly reduced spectral weight of the low-frequency resonance close to the chemical potential requires additional spectral weight at high energies, a consequence of the sum-rule conserving algorithm.

Particle–hole asymmetric spectral functions are displayed in figure 5 for three different values of U. Here, we have chosen the non-interaction resonant-level model $\mathcal{H}^i$ such that the low-temperature fixed-point spectra are identical to those of $\mathcal{H}^f$.

Since the algorithm always evaluates the spectral function at a finite temperature defined by $T_N \propto \Lambda^{-N/2}$ of the last NRG iteration [12, 25, 26, 13] we can also track the temperature evolution of the spectra. For one set of parameters used in figure 5, such a temperature evolution of the steady-state spectra is shown in figure 6. Dashed and solid lines of equal color (color online) correspond to the same temperature. Figure 6 clearly demonstrates that the steady-state algorithm can be used for the temperature evolution of spectral functions as well.

4. Conclusion and outlook

We have presented a new algorithm to calculate non-equilibrium Green functions $G(t, t')$ for quantum impurity models. It is derived using the complete basis set for the Wilson NRG chain [14, 15]. Therefore, the spectral sum-rule is always fulfilled exactly, independent of the number N_s of kept states

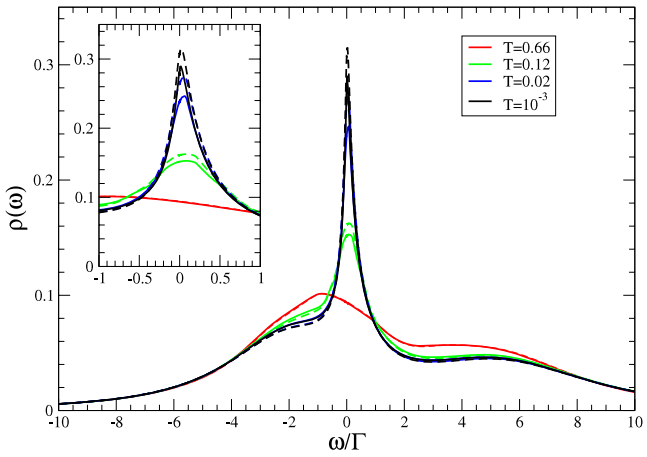

Figure 6. Comparison of the steady-state spectra (solid line) for a fixed value of $U = 8$ and $\epsilon_f = -2.4$ evolved from $U = 0$ and the thermodynamic equilibrium spectra (dashed line) for different values of the temperature $T/\Gamma = 0.66, 0.12, 0.02, 10^{-3}$. The initial level position ϵ_f has been set to $\epsilon_f^i/\Gamma = 0.175$. The black dashed line shows the equilibrium NRG spectra for the small parameters as $\mathcal{H}^f$. The inset shows the resonance in the vicinity of the chemical potential. NRG parameters: as in figure 1.

after each NRG iteration. We have shown that the algorithm for calculating equilibrium spectral functions [17, 18] is included in our approach for the case of an unaltered Hamiltonian $\mathcal{H}^i = \mathcal{H}^f$.

We believe, that this algorithm will open new doors for theoretical calculations of non-equilibrium quantum systems. In another publication [19], we have applied our method to a non-equilibrium problem for which the answer is not known *a priori*: an open quantum system comprising of a quantum dot coupled to two leads whose chemical potential difference drives a current through this interacting junction. Only for the non-interacting problem ($U = 0$) is the exact solution known [21]. However, by switching on the full Coulomb repulsion $\mathcal{H}_U$ at finite bias, the steady-state non-equilibrium spectral function evolves from this initially known solution. The steady-state currents through an interacting nanodevice are accessible to the numerical renormalization group method in the strong-coupling regime at finite bias. This method has the advantage that it is applicable to any arbitrary coupling strength, magnetic field and temperature. In contrast to perturbative approaches it allows the study of the crossover from the weak-coupling regime at high temperatures to the strong-coupling regime at low temperatures and finite bias.

In this paper, we have restricted ourselves to the relevant case of switching on a finite Coulomb repulsion U at $t' = 0$. Focusing on the steady-state limit $t' \to \infty$, we used the well studied equilibrium spectral functions of the SIAM as a benchmark for the steady-stated spectra obtained with our method. Since a closed quantum impurity system will evolve into its thermodynamic equilibrium [24], only if $\mathcal{H}_{\rm imp} + \mathcal{H}_I$ is changed, the deviation between the steady-state and the equilibrium spectra serves as a measure for the quality of the algorithm.

We have shown that the steady-state spectral functions agree excellently with the corresponding equilibrium spectra even at finite magnetic field. The absorbing of the Hartree term into the non-interacting part of the Hamiltonian yields the best agreement between the steady-state spectra and the equilibrium NRG spectra directly obtained from $\mathcal{H}^f$. The singly peaked spectrum of the resonant-level model evolves into the typical three-peak structure of the SIAM in the Kondo regime, with the lower-and high-frequency peaks resulting from charge fluctuations and a narrow many-body Kondo resonance emerging close to the chemical potential whose width is proportional to the correct low-energy scale.

Acknowledgments

We acknowledge discussions with N Andrei, R Bulla, G Czycholl, M Jarrell, Th Costi, N Grewe, H Monien, A Millis, T Novotny, J Kroha, Th Pruschke, A Schiller, P Schmitteckert, A Weichselbaum, and J von Delft, and the KITP, where some of the work was carried out, for its hospitality. This research was supported in part by the DFG projects AN 275/5-1 and AN 275/6-1 and by the National Science Foundation under Grant No. PHY05-51164 (FBA). We acknowledge supercomputer support by the NIC, Forschungszentrum Jülich under project No. HHB000 (FBA).

References

[1] Hewson A C 1993 *The Kondo Problem to Heavy Fermions* (Cambridge: Cambridge University Press)
[2] Leggett A J, Chakravarty S, Dorsey A T and Fisher M P A 1987 *Rev. Mod. Phys.* **59** 1
[3] Kastner M A 1992 *Rev. Mod. Phys.* **64** 849
[4] Goldhaber-Gordon D, Shtrikman H, Mahalu D, Abusch-Magder D, Meirav U and Kastner M 1998 *Nature* **391** 156
[5] Manoharan H C, Lutz C P and Eigler D M 2000 *Nature* **403** 512
[6] Agam O and Schiller A 2001 *Phys. Rev. Lett.* **86** 484
[7] Pruschke Th, Jarrell M and Freericks J K 1995 *Adv. Phys.* **44** 187
[8] Georges A, Kotliar G, Krauth W and Rozenberg M J 1996 *Rev. Mod. Phys.* **68** 13 for a review on the DMFT
[9] Maier T, Jarrell M, Pruschke T and Hettler M H 2005 *Rev. Mod. Phys.* **77** 1027
[10] Kadanoff L P and Baym G 1962 *Quantum Statistical Mechanics* (New York: Benjamin)
[11] Keldysh L V 1965 *Sov. Phys.—JETP* **20** 1018
[12] Wilson K G 1975 *Rev. Mod. Phys.* **47** 773
[13] Bulla R, Costi T and Pruschke T 2008 *Rev. Mod. Phys.* **80** 395
[14] Anders F B and Schiller A 2005 *Phys. Rev. Lett.* **95** 196801
[15] Anders F B and Schiller A 2006 *Phys. Rev.* B **74** 245113
[16] Costi T A 1997 *Phys. Rev.* B **55** 3003
[17] Weichselbaum A and von Delft J 2007 *Phys. Rev. Lett.* **99** 076402
[18] Peters R, Pruschke T and Anders F B 2006 *Phys. Rev.* B **74** 245114
[19] Anders F B 2008 *Preprint* 0802.0371
[20] Meir Y and Wingreen N S 1992 *Phys. Rev. Lett.* **68** 2512
[21] Hershfield S 1993 *Phys. Rev. Lett.* **70** 2134
[22] Oguri A 2007 *Phys. Rev.* B **75** 035302
[23] Doyon B 2007 *Phys. Rev. Lett.* **99** 076806
[24] Doyon B and Andrei N 2006 *Phys. Rev.* B **73** 245326

[25] Krishna-murthy H R, Wilkins J W and Wilson K G 1980 *Phys. Rev.* B **21** 1003
[26] Krishna-murthy H R, Wilkins J W and Wilson K G 1980 *Phys. Rev.* B **21** 1044
[27] Yamada K 1974 *Prog. Theor. Phys.* **53** 970
[28] Yamada K 1975 *Prog. Theor. Phys.* **54** 316
[29] Yamada K and Yoshida K M 1978 *Prog. Theor. Phys.* **59** 1061
[30] Kondo J 1962 *Prog. Theor. Phys.* **28** 864
[31] Anders F B 2005 *Phys. Rev.* B **71** 121101
[32] Cragg D M and Lloyd P 1979 *J. Phys. C: Solid State Phys.* **12** 3301
[33] Pang H B and Cox D L 1991 *Phys. Rev.* B **44** 9454
[34] Bulla R, Tong N and Vojta M 2003 *Phys. Rev. Lett.* **91** 170601
[35] Bulla R, Lee H J, Tong N H and Vojta M 2005 *Phys. Rev.* B **71** 045122
[36] Anders F B, Bulla R and Vojta M 2007 *Phys. Rev. Lett.* **98** 210402
[37] Glossop M T and Ingersent K 2005 *Phys. Rev. Lett.* **95** 67202
[38] Costi T A, Hewson A C and Zlatic V 1994 *J. Phys.: Condens. Matter* **6** 2519
[39] Bulla R, Hewson A C and Pruschke T 1998 *J. Phys.: Condens. Matter* **10** 8365
[40] Bulla R, Costi T A and Vollhardt D 2001 *Phys. Rev.* B **64** 045103
[41] Anderson P W 1961 *Phys. Rev.* **124** 41
[42] Sakai O, Shimizu Y and Kasuya T 1989 *J. Phys. Soc. Japan* **58** 3666
[43] Langreth D C 1966 *Phys. Rev.* **150** 516–8
[44] Anders F B, Grewe N and Lorek A 1991 *Z. Phys.* B **54** 293